C. Numerical Example

A nonlinear capacitance of the Schottky barrier is taken with the

$$Q = \sqrt{2\epsilon q N_d (V_0 - V)} \tag{23}$$

numerical example: $Q = 2.06 \times 10^{-12} \sqrt{0.5 - V}$ biased at $V = -10$ V at 10 GHz.

IV. Conclusion

A definition of the nonlinear reflection coefficient based on the application of the describing function to the power waves has been proposed in this short paper.

Care must be taken to determine in a circuit configuration which is the input waveform: sinusoïdal input current, sinusoïdal input voltage, or sinusoïdal incident wave. As shown in the example, discrepancies might arise between different cases. As we have investigated by computer simulation for nonlinear elements with odd symmetry about the operating point, these discrepancies are small, while for nonlinear elements without symmetry (tunnel diode in the example) they are quite important. This concludes that while working on a network analyzer one might interchange nonlinear resistance and nonlinear reflection coefficient concepts in the first case, while in the latter case nonlinear reflection coefficient on a $b-a$ linearization basis should be used, provided "b" harmonics are loaded by the characteristic impedance.

References

[1] A. Blaquiere, *Nonlinear System Analysis*. New York: Academy Press, 1966.

[2] W. Vandervelde and A. Gelb, *Multiple Input Describing Functions and Nonlinear System Design*. New York: McGraw-Hill, 1968.

[3] C. W. Lee, "Highpower negative resistance amplifier," *Microwave J.*, Feb. 1972.

[4] D. J. Esdale and M. J. Howes, "A reflection coefficient approach to the design of one-port negative impedance oscillators," *IEEE Trans. Microwave Theory Tech.*, vol. MTT-29, Aug. 1981.

[5] Hewlett-Packard, "*S*-parameters, circuit analysis and design," Appl. Note 95, Palo Alto, CA, Sept. 1968.

[6] E. S. Kuh and R. A. Rohrer, *Theory of Linear Active Network*. Oakland, CA: Holden-Day, 1967

Application of Boundary-Element Method to Electromagnetic Field Problems

SHIN KAGAMI AND ICHIRO FUKAI

Abstract—**This paper proposes an application of the boundary-element method to two-dimensional electromagnetic field problems. By this method, calculations can be performed using far fewer nodes than by the finite-element method, and unbounded field problems are easily treated without special additional consideration. In addition, the results obtained have fairly good accuracy. In this paper, analyzing procedures of electromagnetic field problems by the boundary-element method, under special conditions, are proposed and several examples are investigated.**

Manuscript received April 15, 1983; revised October 12, 1983.

S. Kagami is with the Department of Electrical Engineering, Asahikawa Technical College, Asahikawa, Japan 070.

I. Fukai is with the Department of Electrical Engineering, Faculty of Engineering, Hokkaido University, Sapporo, Japan 060.

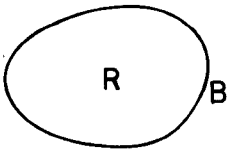

Fig. 1. Two-dimensional region R.

I. Introduction

At present, the finite-element method is widely used in many fields. The main reason may be that, by the finite-element method, it is easy to handle inhomogeneities and complicated structures. However, it requires a large computer memory and long computing time to solve the final matrix equation. In addition, unbounded field problems need some additional techniques [1], [2].

Recently, the boundary-element method has been proposed, which is interpreted as a combination technique of the conventional boundary-integral equation method and a discretization technique, such as the finite-element method, and which has merits of both the above methods, i.e., the required size of the computer memory being small and the obtained results having fairly good accuracy [3], [4]. Namely, the boundary-element method is a boundary method and, therefore, if the region to be analyzed is homogeneous, then it requires nodes, necessary for calculation, on its boundary only. So the problem can be treated with one less dimension. Moreover, it can handle unbounded field problems easily, so that it is suitable for the electromagnetic field analysis which often includes unbounded regions [5], [6].

In this paper, a formulation of two-dimensional electromagnetic field problems by the boundary-element method and its application to several interesting cases, such as the problem of electromagnetic waveguide discontinuities, multi-media problems, and electromagnetic wave scattering problems [6]. In addition, several examples are analyzed and the results obtained with the boundary-element method are compared with rigorous ones, and solutions of the other numerical methods. The propriety of our analyzing procedure of the boundary-element method is verified.

II. General Formulation

A two-dimensional region R enclosed by a boundary B, as illustrated in Fig. 1, is considered. In the region R, Helmholtz's equation

$$(\nabla^2 + k^2) u = 0 \tag{1}$$

holds, where u is the potential used for analysis, we write its outward normal derivative as q, and k denotes the wavenumber in free space. The boundary condition on B is

$$u = \bar{u} \tag{2}$$

or

$$q = \bar{q} \tag{3}$$

where "$\bar{}$" means a known value. Here, Green's function

$$u^* = -\frac{j}{4} H_0^{(2)}(kr) \tag{4}$$

is introduced, where $H_0^{(2)}$ is the Hankel function of the second kind and order zero. By the method of weighted residuals [3], [4] or Green's formula, the following equation is obtained:

$$u_i + \int_B u q^* \, dc = \int_B q u^* \, dc. \tag{5}$$

0018-9480/84/0400-0455$01.00 ©1984 IEEE

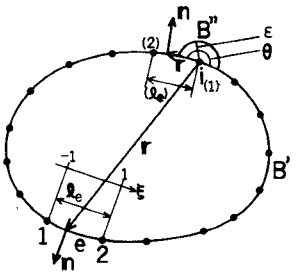

Fig. 2. Integration on each element.

In (5), the suffix "i" means an arbitrary point in the region R and q^* is the outward normal derivative of u^*

$$q^* = \frac{j}{4} H_1^{(2)}(kr) \frac{\partial (kr)}{\partial n} = \frac{j}{4} k H_1^{(2)}(kr) \cos\angle(\boldsymbol{r}; \boldsymbol{n}). \tag{6}$$

In (6), $H_1^{(2)}$ is the Hankel function of the second kind and order one. For the case where the point i is placed on the boundary B, the singular point of Green's function appears and special consideration is necessary. Now, we adopt the integration path going round the node i as shown in Fig. 2. Then, (5) is rewritten as follows:

$$u_i + \lim_{\epsilon \to 0} \int_{B'} uq^* \, dc + \lim_{\epsilon \to 0} \int_{B''} uq^* \, dc = \lim_{\epsilon \to 0} \int_{B'} qu^* \, dc + \lim_{\epsilon \to 0} \int_{B''} qu^* \, dc. \tag{7}$$

Here, we estimate the integration over the boundary B'' as follows:

$$\begin{aligned} \lim_{\epsilon \to 0} \int_{B''} uq^* \, dc &= \lim_{\epsilon \to 0} \int_{B''} u \frac{j}{4} k H_1^{(2)}(k\epsilon) \, dc \\ &= \lim_{\epsilon \to 0} u \frac{j}{4} k H_1^{(2)}(k\epsilon) \epsilon\theta \\ &= \frac{j}{4} k\theta \lim_{\epsilon \to 0} \left[\epsilon \left\{ \frac{k\epsilon}{2} - j\left(-\frac{2}{\pi} \frac{1}{k\epsilon} \right) \right\} \right] \\ &= -\frac{\theta}{2\pi} u_i \end{aligned} \tag{8}$$

$$\begin{aligned} \lim_{\epsilon \to 0} \int_{B''} qu^* \, dc &= \lim_{\epsilon \to 0} \int_{B''} q \left\{ -\frac{j}{4} H_0^{(2)}(k\epsilon) \right\} dc \\ &= \lim_{\epsilon \to 0} \left[q\left(-\frac{j}{4} \right) \left\{ 1 - j\frac{2}{\pi} (\ln k\epsilon + \gamma - \ln 2) \right\} \epsilon\theta \right] \\ &= 0 \end{aligned}$$

$$\gamma = 0.5772 \cdots \quad \text{(Euler's number)}. \tag{9}$$

From (5), (8), and (9), we derive the next equation as follows:

$$c_i u_i + \int_B qu^* \, dc = \int_B qu^* \, dc,$$

$$c_i = 1 - \frac{\theta}{2\pi} \qquad \int_B = \lim_{\epsilon \to 0} \int_{B'}. \tag{10}$$

In (10), $\int$ denotes the Cauchy's principal value of integration. Next, the boundary B is approximated by the connection of line elements, on each of which u and q are assumed to vary linearly. Then, (10) is discretized as follows:

$$c_i u_i + \sum_{e=1}^{n} [h_1 h_2]_e \begin{Bmatrix} u_1 \\ u_2 \end{Bmatrix}_e = \sum_{e=1}^{n} [g_1 g_2]_e \begin{Bmatrix} q_1 \\ q_2 \end{Bmatrix}_e. \tag{11}$$

In (11), n is the number of elements and u_1, u_2, q_1, and q_2 are the potentials and the potential derivatives on the two nodes of the eth element and h_1, h_2, g_1, and g_2 are contributions of the eth element to integration. When the point i does not belong to the eth element, they are calculated with Gaussian integration as

$$\begin{Bmatrix} h_1 \\ h_2 \end{Bmatrix} = \int_{-1}^{1} \begin{Bmatrix} \phi_1 \\ \phi_2 \end{Bmatrix} \frac{1}{4} jk H_1^{(2)}(kr) \cos\angle(\boldsymbol{r}; \boldsymbol{n}) \, d\xi \cdot \frac{1}{2} l_e \tag{12}$$

$$\begin{Bmatrix} g_1 \\ g_2 \end{Bmatrix} = \int_{-1}^{1} \begin{Bmatrix} \phi_1 \\ \phi_2 \end{Bmatrix} \left\{ -\frac{1}{4} jH_0^{(2)}(kr) \right\} d\xi \cdot \frac{1}{2} l_e \tag{13}$$

where ξ is a normalized coordinate defined on the eth element, l_e is the length of the element, and ϕ_1 and ϕ_2 are the interpolation functions given as follows:

$$\begin{Bmatrix} \Phi_1 \\ \Phi_2 \end{Bmatrix} = \frac{1}{2}(1 \mp \xi). \tag{14}$$

When the point i belongs to the eth element, calculations of g_1, g_2, h_1, and h_2 involve the limitation of $\epsilon \to 0$. In this case, the vector $\boldsymbol{r}$ is at right angles to the outward normal vector $\boldsymbol{n}$ (see Fig. 2), so that $\cos(\boldsymbol{r}; \boldsymbol{n})$ becomes equal to zero and

$$h_1 = h_2 = 0. \tag{15}$$

The remainders are g_1 and g_2. Here, we consider the case where the point i coincides with the first node of the eth element

$$\begin{aligned} g_1 &= \lim_{\epsilon \to 0} \int_{-1+\epsilon}^{1} \frac{1}{2}(1-\xi) \left\{ -\frac{1}{4} jH_0^{(2)}(kr) \right\} d\xi \cdot \frac{1}{2} l_e \\ &= \frac{jl_e}{16} \lim_{\epsilon \to 0} \int_{-1+\epsilon}^{1} (\xi - 1) H_0^{(2)} \left\{ k(\xi+1) \frac{1}{2} l_e \right\} d\xi \\ &= \frac{jl_e}{16} \lim_{\epsilon \to 0} \int_{\epsilon}^{2} \left\{ \xi H_0^{(2)}\left(k\xi \cdot \frac{1}{2} l_e \right) - 2H_0^{(2)}\left(k\xi \cdot \frac{1}{2} l_e \right) \right\} d\xi \\ &= \frac{jl_e}{16} \lim_{\epsilon \to 0} \left\{ \left[\frac{2\xi}{kl_e} H_1^{(2)}\left(\frac{1}{2} kl_e \xi \right) \right]^2 - 2 \int^2 H_0^{(2)}\left(\frac{1}{2} kl_e \xi \right) d\xi \right\}. \end{aligned} \tag{16}$$

In the second term of (16), the Hankel function is expanded to infinite series and is integrated by term

$$g_1 = \frac{1}{4} jl_e \left[\frac{1}{kl_e} H_1^{(2)}(kl_e) + j\frac{2}{\pi} \left\{ \ln\left(\frac{1}{2} kl_e \right) + \gamma - 1 - \left(\frac{1}{kl_e} \right)^2 \right\} - 1 - \sum_{s=1}^{\infty} \frac{(-1)^s (kl_e)^{2s}}{(s!)^2 2^{2s} (2s+1)} \left\{ 1 - j\frac{2}{\pi} \left(\ln \frac{kl_e}{2} + \gamma - h_s - \frac{1}{2s+1} \right) \right\} \right]$$

$$h_s = 1 + \frac{1}{2} + \frac{1}{3} + \cdots + \frac{1}{s}. \tag{17}$$

From (16) and (17), we obtain the next result for g_2

$$g_2 = -\frac{1}{4} jl_e \left[\frac{1}{kl_e} H_1^{(2)}(kl_e) - j\frac{2}{\pi} \left(\frac{1}{kl_e} \right)^2 \right]. \tag{18}$$

If the point i is the second node of the eth element, then g_1 is estimated with (18) and g_2 with (17). The infinite series in (17) is approximated by the first few terms, since the length of the eth element l_e is chosen as $l_e < \lambda/10$, i.e., $kl_e < 2\pi/10$, so that the series rapidly converges, where λ is the wavelength in free space.

In the above calculations, the estimation of c_i is important for the Dirichlet boundary condition giving the nonzero potential. Because c_i is the coefficient of u_i, any value of c_i is permitted for the boundary condition giving the zero potential; but for the case of the nonzero potential, c_i must be calculated precisely [7].

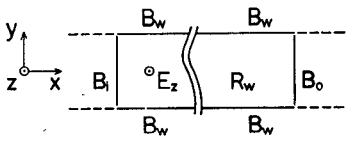

Fig. 3. A parallel-plane waveguide with discontinuities.

In the matrix notation, (11) is rewritten as follows:

$$\boldsymbol{H}\boldsymbol{u} = \boldsymbol{G}\boldsymbol{q}. \tag{19}$$

On each node, the potential u or its outward normal derivative q must be given as the boundary condition. Then, all the remaining u's and q's can be calculated from (19). The matrices produced by the boundary-element formulation are much smaller in size than the finite-element method.

III. The Case of Waveguides with Discontinuities

For a typical example, a parallel-plane waveguide with discontinuities is considered, and the mode having the z-component of the electric field, which is chosen as the analyzed potential u, is assumed. In this case, a closed region R_w, as shown in Fig. 3, is chosen as the analyzed model, which is enclosed by the boundary of the waveguide wall B_w and pseudo-boundaries at the power supply side and the opposite load side, which we call the input-side boundary B_i and the output-side boundary B_o, respectively.

From (19), the following equation is obtained for the region R_w:

$$[\boldsymbol{H}_i\boldsymbol{H}_o\boldsymbol{H}_w]\begin{Bmatrix}\boldsymbol{u}_i\\ \boldsymbol{u}_o\\ \boldsymbol{u}_w\end{Bmatrix} = [\boldsymbol{G}_i\boldsymbol{G}_o\boldsymbol{G}_w]\begin{Bmatrix}\boldsymbol{q}_i\\ \boldsymbol{q}_o\\ \boldsymbol{q}_w\end{Bmatrix}, \qquad \text{in } R_w. \tag{20}$$

In (20), suffixes i, o, and w show the quantities corresponding to the boundaries B_i, B_o, and B_w, respectively. On the waveguide wall, the electric-field component parallel to it vanishes, so that the following boundary condition is taken:

$$\boldsymbol{u}_w = 0, \qquad \text{on } B_w. \tag{21}$$

But on the remaining boundaries B_i and B_o, any specified value of u or q cannot be given. If they are given, the phase relation between the field components on the input- and the output-side boundaries are also given, and, therefore, the problem has already been solved. This is a contradiction.

Now, we adopt the following procedure. First, we place the two pseudo-boundaries B_i and B_o at the position where it is considered that the reflecting electromagnetic wave, generated at the discontinuites, attenuates and almost vanishes. The TE_{10}-mode field distribution is assumed on them. Then, on only B_i, the boundary condition, in complex form, is placed

$$\boldsymbol{u}_i = \bar{\boldsymbol{u}}_i, \qquad \text{on } B_i. \tag{22}$$

Next, on B_o, we introduce the TE_{10}-mode propagation constant β, and the electric-field component is written as

$$u_o = E_{z0}\exp(-j\beta y), \qquad \text{on } B_o \tag{23}$$

and its outward normal derivative q_o is also written as

$$q_o = \frac{du_o}{dy} = -j\beta E_{z0}\exp(-j\beta y), \qquad \text{on } B_o. \tag{24}$$

So, on B_o, the next relationship between u_o and q_o is obtained as follows:

$$\boldsymbol{q}_o = -j\beta\boldsymbol{u}_0, \qquad \text{on } B_o. \tag{25}$$

From (20), (21), (22), and (25), the following equation, to be solved finally, is obtained:

$$[\boldsymbol{G}_i - j\beta\boldsymbol{F}_o - \boldsymbol{H}_o\boldsymbol{G}_w]\begin{Bmatrix}\boldsymbol{q}_i\\ \boldsymbol{u}_o\\ \boldsymbol{q}_w\end{Bmatrix} = \boldsymbol{H}_i\bar{\boldsymbol{u}}_i, \qquad \text{in } R_w. \tag{26}$$

In the right-hand side of (26), all quantities are known and $\boldsymbol{q}_i$, $\boldsymbol{u}_o$, and $\boldsymbol{q}_w$ are obtained as a solution. Then, $\boldsymbol{q}_o$ is given by (25).

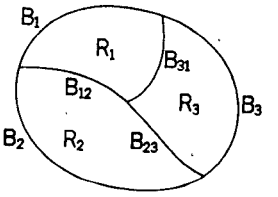

Fig. 4. Two-dimensional region constructed of three media.

IV. Multi-Media Problems

For multi-media cases, any boundary method requires to make up equations for each homogeneous sub-domain constructed of one media. So it is generally said that boundary methods are weak in multi-media problems and the finite-element method is superior to the boundary-element method in such a case. However, the authors have verified that a bit of effort on the design of the computer program makes this fault of the boundary-element method negligible, and they propose a procedure of programming, for handling multi-media problems, in a slightly different style from those of the references [3], [4].

Consider a two-dimensional region constructed of three different media, as shown in Fig. 4, where R_1, R_2, and R_3 are homogeneous sub-domains, B_1, B_2, and B_3 are the boundaries belonging to only R_1, R_2, and R_3, respectively, and B_{12}, B_{23}, and B_{31} are the interfaces between two adjacent sub-domains. The ordinary boundary-element technique leads to the following equations for each homogeneous sub-domain:

$$[\boldsymbol{G}_1\boldsymbol{G}_{12}^{(1)}\boldsymbol{G}_{31}^{(1)}]\begin{Bmatrix}\boldsymbol{q}_1\\ \boldsymbol{q}_{12}^{(1)}\\ \boldsymbol{q}_{31}^{(1)}\end{Bmatrix} = [\boldsymbol{H}_1\boldsymbol{H}_{12}^{(1)}\boldsymbol{H}_{31}^{(1)}]\begin{Bmatrix}\boldsymbol{u}_1\\ \boldsymbol{u}_{12}^{(1)}\\ \boldsymbol{u}_{31}^{(1)}\end{Bmatrix}, \qquad \text{in } R_1 \tag{27}$$

$$[\boldsymbol{G}_2\boldsymbol{G}_{23}^{(2)}\boldsymbol{G}_{12}^{(2)}]\begin{Bmatrix}\boldsymbol{q}_2\\ \boldsymbol{q}_{23}^{(2)}\\ \boldsymbol{q}_{12}^{(2)}\end{Bmatrix} = [\boldsymbol{H}_2\boldsymbol{H}_{23}^{(2)}\boldsymbol{H}_{12}^{(2)}]\begin{Bmatrix}\boldsymbol{u}_2\\ \boldsymbol{u}_{23}^{(2)}\\ \boldsymbol{u}_{12}^{(2)}\end{Bmatrix}, \qquad \text{in } R_2 \tag{28}$$

$$[\boldsymbol{G}_3\boldsymbol{G}_{31}^{(3)}\boldsymbol{G}_{23}^{(3)}]\begin{Bmatrix}\boldsymbol{q}_3\\ \boldsymbol{q}_{31}^{(3)}\\ \boldsymbol{q}_{13}^{(3)}\end{Bmatrix} = [\boldsymbol{H}_3\boldsymbol{H}_{31}^{(3)}\boldsymbol{H}_{13}^{(3)}]\begin{Bmatrix}\boldsymbol{u}_3\\ \boldsymbol{u}_{31}^{(3)}\\ \boldsymbol{u}_{13}^{(3)}\end{Bmatrix}, \qquad \text{in } R_3. \tag{29}$$

In (27)–(29), superscript (i) implies the quantity defined in R_i. The boundry conditions on the interfaces are as follows:

$$\boldsymbol{u}_{12}^{(1)} = \boldsymbol{u}_{12}^{(2)} = \boldsymbol{u}_{12}, \quad \boldsymbol{q}_{12}^{(1)} = -\boldsymbol{q}_{12}^{(2)} = \boldsymbol{q}_{12}, \qquad \text{on } B_{12} \tag{30}$$

$$\boldsymbol{u}_{23}^{(2)} = \boldsymbol{u}_{23}^{(3)} = \boldsymbol{u}_{23}, \quad \boldsymbol{q}_{23}^{(2)} = -\boldsymbol{q}_{23}^{(3)} = \boldsymbol{q}_{23}, \qquad \text{on } B_{23} \tag{31}$$

$$\boldsymbol{u}_{31}^{(3)} = \boldsymbol{u}_{31}^{(1)} = \boldsymbol{u}_{31}, \quad \boldsymbol{q}_{31}^{(3)} = -\boldsymbol{q}_{31}^{(1)} = \boldsymbol{q}_{31}, \qquad \text{on } B_{31}. \tag{32}$$

In the above conditions, the minus sign of q originates from the outward normal directions of the adjacent two subregions opposite each other. From (27)–(32), we obtain the next equation to

be solved finally.

$$\begin{bmatrix} G_1 & O & O & G_{12}^{(1)} & -H_{12}^{(1)} & O & O & -G_{31}^{(1)} & -H_{31}^{(1)} \\ O & G_2 & O & -G_{12}^{(2)} & -H_{12}^{(2)} & G_{23}^{(2)} & -H_{23}^{(2)} & O & O \\ O & O & G_3 & O & O & -G_{23}^{(3)} & -H_{23}^{(3)} & G_{31}^{(3)} & H_{31}^{(3)} \end{bmatrix} \begin{bmatrix} q_1 \\ q_2 \\ q_3 \\ q_{12} \\ u_{12} \\ q_{23} \\ u_{23} \\ q_{31} \\ u_{31} \end{bmatrix} = \begin{bmatrix} H_1 & O & O \\ O & H_2 & O \\ O & O & H_3 \end{bmatrix} \begin{bmatrix} u_1 \\ u_2 \\ u_3 \end{bmatrix}, \quad \text{in } R_1 + R_2 + R_3. \tag{33}$$

V. Electromagnetic Scattering Problems

In this section, the procedure analyzing the problem of electromagnetic scattering by dielectric bodies is developed. This is considered to be the problem of multi-media and the unbounded field. Therefore, the procedure developed for multi-media problems can be utilized for the scattering problem in the form extended a little.

It is assumed that the incident wave is the E-wave and propagates in the direction parallel to the $x-y$ plane. All quantities are uniform in the z-direction. The analyzed region is constructed of two subregions, as shown in Fig. 5. Subregion R_I is inside the dielectric cylinder and subregion R_O is outside of it. The latter is an unbounded field, but at infinity, the radiation condition can be taken for the scattering wave, so that the boundary-element equations are considered on only the dielectric surface B_d

$$\begin{aligned} G_I q_I &= H_I u_I, \qquad \text{in } R_I \\ u_I &= u_{I,sc} + u_{I,in} \\ q_I &= q_{I,sc} + q_{I,in} \end{aligned} \tag{34}$$

$$G_O q_{O,sc} = H_O u_{O,sc}, \qquad \text{in } R_O. \tag{35}$$

Here, subscripts I and O imply the quantities defined in R_I and R_O, respectively, and sc and in indicate the scattering and incident waves, respectively. In R_I, the ruling equation is defined using the total wave, i.e., the incident wave plus the scattering wave. On the contrary, in R_O, the radiation condition can't be applied for the incident wave, so that the equation is defined by only the scattering wave.

On B_d, the following boundary conditions are taken:

$$u_{I,sc} = u_{O,sc} = u_{sc}, \qquad \text{on } B_d \tag{36}$$

$$q_{I,sc} = -q_{O,sc} = q_{sc}, \qquad \text{on } B_d. \tag{37}$$

In addition, the incident wave is described as follows:

$$u_{in} = u_{I,in} = E_{z_0,in} \exp(jk\rho). \tag{38}$$

Here, the ρ coordinate is chosen in the direction of the incidence, as in Fig. 5. For $q_{I,in}$, we derive the following equation:

$$\begin{aligned} q_{I,in} &= \frac{du_{I,in}}{dn_I} = -jk\boldsymbol{n}_I \cdot \boldsymbol{n}_\rho u_{I,in} \\ &= x\cos\theta + y\sin\theta \end{aligned} \tag{39}$$

where θ is the incident angle. In matrix notation, the above relation is rewritten as

$$q_{I,in} = B_I u_{I,in}. \tag{40}$$

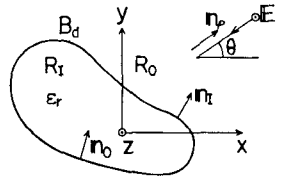

Fig. 5. Electromagnetic scattering by a dielectric cylinder.

From (34)–(40), the following equation is obtained for $R_I + R_O$:

$$\begin{bmatrix} -G_I & H_I \\ G_O & -H_O \end{bmatrix} \begin{bmatrix} u_{sc} \\ q_{sc} \end{bmatrix} = \begin{bmatrix} H_I - G_I B_I \\ O \end{bmatrix} u_{I,in}. \tag{41}$$

By (41), the scattering field is calculated on the boundary B_d provided that the incident wave is given there.

The procedure proposed here is very powerful for the case where the dielectric body has a much larger dimension than the wavelength of the incidence or has a large dielectric constant. The finite-element method is weak because it requires a large computer memory.

VI. Analyzed Results

A. Open-Ended Parallel-Plane Waveguides

We analyzed the reflection coefficients of three kinds of waveguides, i.e., flanged, unflanged, and flared, consisting of two parallel planes. These are unbounded field problems, and closed boundaries extending to infinity should be chosen. But at infinity, the radiation condition can be introduced, and at the point several wavelengths distant from the open-end of the waveguide, the field value becomes negligibly small, so that the contribution to the integration can be neglected. The finite models are chosen as in Fig. 6, which are half-models, because each of them has the symmetry axis parallel to the direction of electromagnetic wave propagation. Fig. 7 denotes the results obtained with the boundary-element method for the above three cases. They have good agreement with Lee's solution by ray theory [8], Vaynshteyn's by the Wiener-Hopf technique [9], and the results by the finite-element method extended to unbounded fields [2]. For the flared waveguide, the boundary-element method results are compared with those of the boundary integral equation method [10]. All of the above boundary-element calculations are performed with 40 nodes, while the corresponding finite-element calculations need at least 400 nodes. The problems analyzed here are unbounded ones, for which the boundary-element method seems to be the most suitable method.

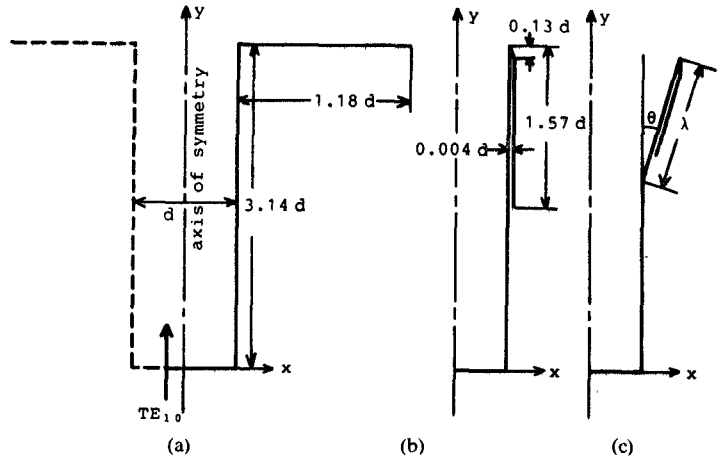

Fig. 6. Analyzed models of open-ended parallel-plane waveguides. (a) Flanged, (b) unflanged, and (c) flared.

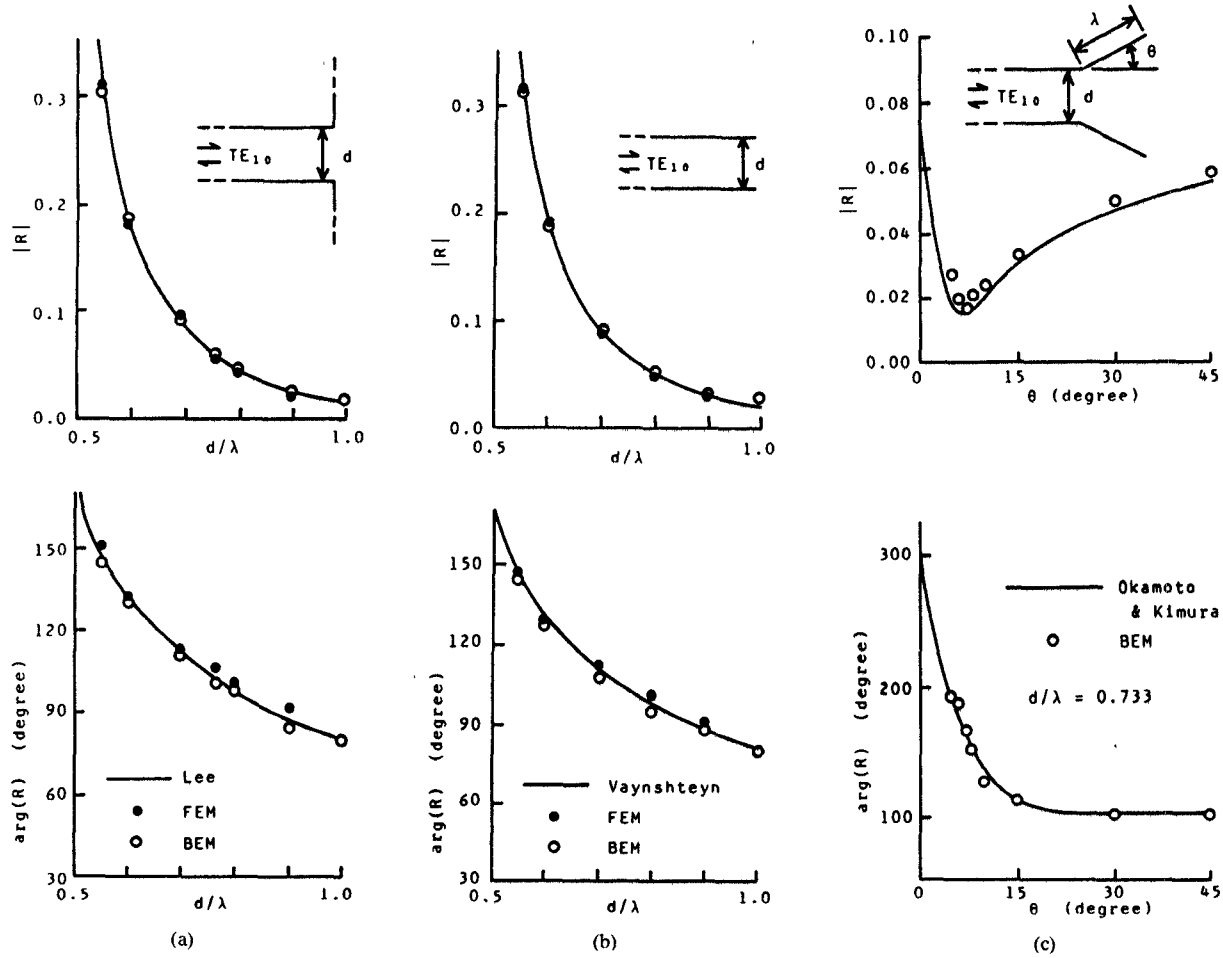

Fig. 7. Reflection coefficients of open-ended parallel-plane waveguides. Absolute value $|R|$ and phase $\arg(R)$. (a) Flanged, (b) unflanged, and (c) flared.

B. A Symmetrical H-Plane Y-Junction

The electric-field distribution in an *H*-plane Y-junction is analyzed. The electromagnetic wave is assumed to propagate along the *y*-axis, as in Fig. 8, which also indicates the analyzed model. The right half of the model is considered for the symmetry. On the input- and output-side boundaries, the TE_{10} mode is assumed. Fig. 9 shows the electric-field distribution, represented by the standing-wave on the centerlines. Details of their positions are shown in Fig. 8. From the results in Fig. 8, the reflection coefficient due to this Y-junction is calculated as 0.18. This value leads to the calculated amplitude of the electric field at the output side of the junction, $\sqrt{(1-0.18^2)/2} = 0.6956$, where that of the input side is assumed to be 1.0. The value, 0.6956, agrees well with the boundary-element result of the electric standing-wave amplitude in Fig. 9.

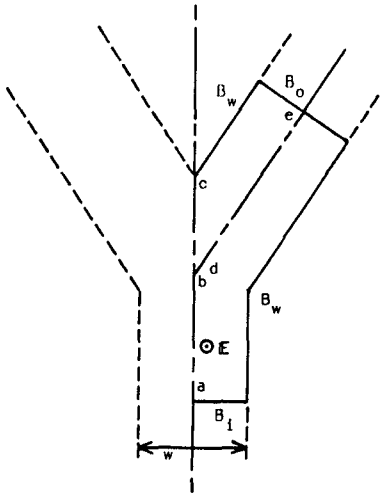

Fig. 8. Analyzed model of H-plane Y-junction.

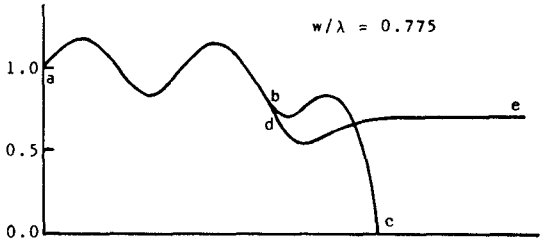

Fig. 9. The electric-field distribution in a H-plane Y-junction.

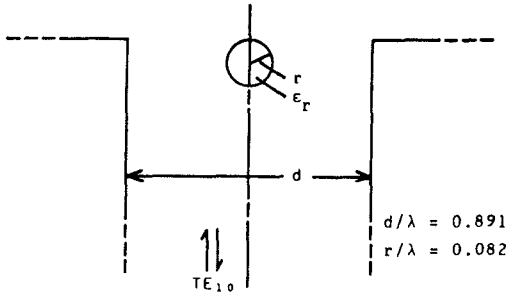

Fig. 10. Flanged open-ended waveguide with a dielectric cylinder placed at its open-end.

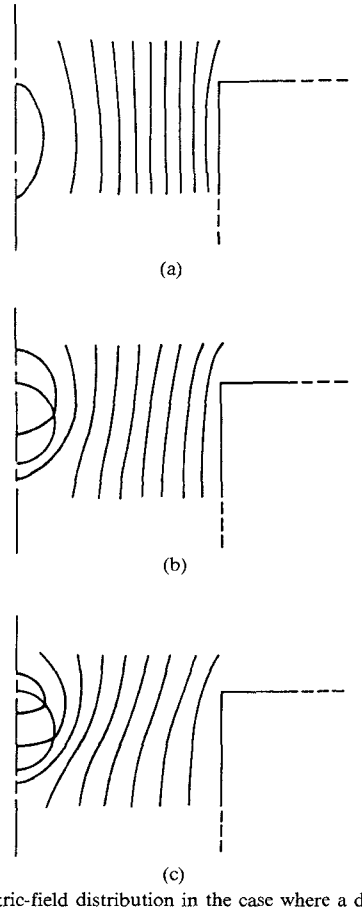

Fig. 11. The electric-field distribution in the case where a dielectric cylinder is placed at the open-end of flanged waveguides. (a) Dielectric constant of the cylinder $\epsilon_r = 1.0$, i e., no cylinder is placed. (b) $\epsilon_r = 2.0$. (c) $\epsilon_r = 3\,0$.

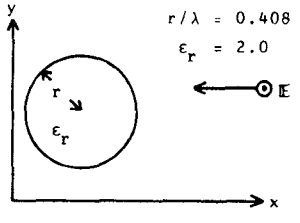

Fig. 12. Dielectric circular cylinder and the incident E-wave.

C. A Waveguide with a Dielectric Cylinder Placed at its Open-end

Here, we analyze the electromagnetic-field distribution of the case where the parallel-plane waveguide is open-ended with infinite flanges and a dielectric cylinder is placed at the open-end, as in Fig. 10. Fig. 11 shows the electric-field distributions for three values of dielectric constant, 1.0, 2.0, and 3.0. The case where $\epsilon_r = 1.0$ implies a homogeneous case, i.e., no cylinder is placed. This model brings the reflection coefficient, 0.029, which agrees with that obtained by the computer program for the homogeneous case (cf. Fig. 7(a)) and clarifies the propriety of the multi-media case analyzing procedure. From Fig. 11, it is found that the larger dielectric constant becomes, the denser the electric-field concentrates to the dielectric cylinder.

D. Electromagnetic Scattering of Dielectric Circular Cylinder

As the last example, the plane electromagnetic wave scattering by a dielectric circular cylinder is investigated. The incident wave is assumed to travel along the x-axis in the negative x-direction. Details are shown in Fig. 12. The dielectric cylinder is assumed to have a dielectric constant 2.0 and a radius 0.408λ, where λ is a wavelength in free space. Fig. 13 is the amplitude and phase of the E-wave scattering far-field pattern in this case. In addition, Fig. 14 shows the electric-field distribution around the dielectric cylinder. In Fig. 13, the results obtained by the boundary-element method are compared with analytical ones and show good accuracy. The calculations are done with only 24 nodes. For smaller cylinders, more accurate results have been obtained. For larger cylinders, no actual analysis has yet been performed, but it seems that the boundary-element method is more suitable than the finite-element method.

E. Computer Implementation

Boundary-element calculations require only a small computer memory, so that a microcomputer can handle them. The techniques discussed in this paper have been implemented by a

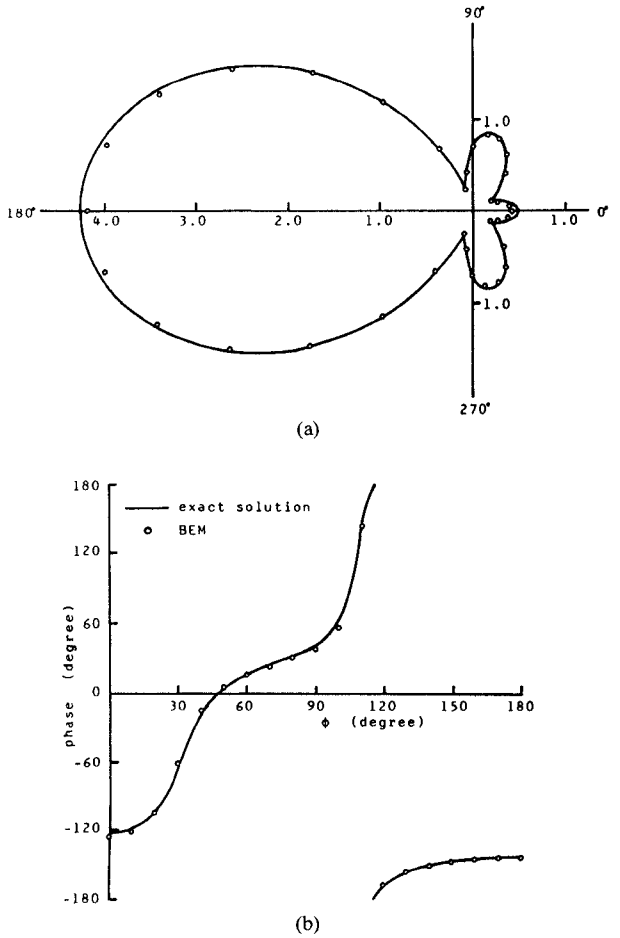

Fig. 13. E-wave scattering far-field pattern for dielectric circular cylinder in the case where E-wave incidents along x-axis in the negative x-direction. (a) Amplitude. (b) Phase.

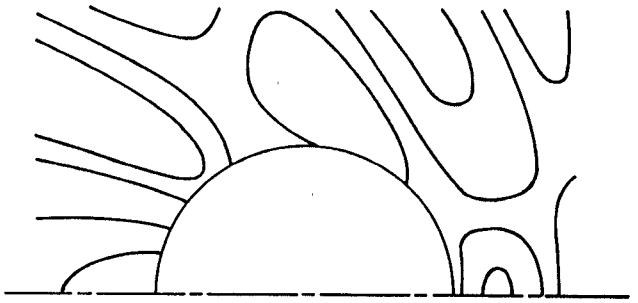

Fig. 14. The electric-field distribution around the dielectric circular cylinder.

FORTRAN program on a microcomputer, whose main CPU is MC68000 (8 MHz) and whose operating system is the UCSD p-system. Typically, the case of a parallel-plane waveguide having 40 nodes took about 20 m of CPU time.

VII. Conclusions

Application of the boundary-element method to electromagnetic-field problems was proposed. Several analyzing procedures for interesting cases were also given. The results obtained show that the boundary-element method is a very powerful numerical method for electromagnetic-field problems. Namely, by using the boundary-element method, far fewer nodes than by the finite-element method bring good accuracy, and unbounded field problems can be treated without any additional technique.

References

[1] B. H. McDonald and A. Wexler, "Finite-element solution of unbounded field problems," *IEEE Trans Microwave Theory Tech*, vol MTT-20, pp. 841–847, Dec. 1972.
[2] S. Washisu, I. Fukai, and M. Suzuki, "Extension of finite-element method to unbounded field problems," *Electron. Lett.*, vol. 15, pp 772–774, Nov. 1979.
[3] C A. Brebbia, *The Boundary Element Method for Engineers*. London: Pentech Press, 1978.
[4] C. A. Brebbia and S. Walker, *Boundary Element Techniques in Engineering*. London: Butterworth, 1980.
[5] S. Washisu and I. Fukai, "An analysis of electromagnetic unbounded field problems by boundary element method," *Trans. Inst. Electron. Commun. Eng. Jpn.*, vol. J64-B, pp. 1359–1365, Dec. 1981.
[6] S. Bilgen and A. Wexler, "Spline boundary element solution of dielectric scattering problems," in *12th Eur. Microwave Conf.*, (Helsinki, Finland), Sept. 1982, pp. 372–377.
[7] C. G. Williams and G. K. Cambrell, "Efficient numerical solution of unbounded field problems," *Electron. Lett.*, vol. 8, pp. 247–248, May 1972.
[8] S. W. Lee, "Ray theory of diffraction by open-ended waveguides. Part I," *J. Math. Phys.*, vol. 11, pp. 2830–2850, Sept. 1970.
[9] L. A. Vaynshteyn, *The Theory of Diffraction and the Factorization Method*. Boulder, CO: Golem, 1969.
[10] N. Okamoto and T. Kimura, "Radiation properties of H-plane two-dimensional horn antennas of arbitrary shape," *Trans. Inst. Electron. Commun. Eng. Jpn.*, vol. J59-B, pp. 25–32, Jan. 1976.

Optimum Design of a Potentially Dispersion-Free Helical Slow-Wave Circuit of a Broad-Band TWT

B. N. BASU, B. B. PAL, V. N. SINGH, AND N. C. VAIDYA

Abstract—**The results of an equivalent circuit analysis are studied for a potentially dispersion-free slow-wave circuit of a TWT which consists of a dielectric-supported helix in a metal shell provided with vanes. The optimum vane dimensions are predicted, which should be helpful in broadbanding the performance of a TWT.**

I. Introduction

With the advent of multi-octave-band traveling-wave tubes (TWT's), the study of dispersion shaping in the slow-wave structures of such tubes has become important [1]–[3]. In the case of a tube having a metal shell, dispersion can be reduced by placing the shell very close to the helix, but this will reduce the interaction impedance considerably. An alternative method would be to use a shell provided with metal vanes projected radially inward [1], [2]. In this case, the shell can be placed farther from the helix with the metal vanes allowed to approach the helix. The desired flat dispersion characteristics may be obtained by optimizing the radial dimension of the vanes.

In this paper, we present an optimum design curve relating the vane dimension and the location of the metal shell with respect to the helix, for different values of the helix wire radius. The curve is obtained by studying the dispersion relation of the circuit which can be derived using an equivalent circuit analysis.

Manuscript received April 26, 1983; revised October 31, 1983.
The authors are with the Centre of Research in Microwave Tubes, Department of Electronic Engineering, Institute of Technology, B.H.U., Varanasi-221 005, India

0018-9480/84/0400-0461$01.00 ©1984 IEEE